Colorectal cancer Consensus Molecular Subtypes translated to preclinical models uncover potentially targetable cancer-cell dependencies

Anita Sveen[1,2,*], Jarle Bruun[1,2,3,*], Peter W. Eide[1,2], Ina A. Eilertsen[1,2], Lorena Ramirez[4], Astrid Murumägi[3], Mariliina Arjama[3], Stine A. Danielsen[1,2], Kushtrim Kryeziu[1,2], Elena Elez[4], Josep Tabernero[4], Justin Guinney[5], Hector G. Palmer[4], Arild Nesbakken[2,6,7], Olli Kallioniemi[3], Rodrigo Dienstmann[4,5], Ragnhild A. Lothe[1,2,7,#]

[1]Department of Molecular Oncology, Institute for Cancer Research and [2]K.G.Jebsen Colorectal Cancer Research Centre, Oslo University Hospital, Oslo, Norway

[3]Institute for Molecular Medicine Finland (FIMM), University of Helsinki, Helsinki, Finland

[4]Vall d'Hebron University Hospital and Institute of Oncology (VHIO), Universitat Autònoma de Barcelona, CIBERONC, Barcelona, Spain

[5]SAGE Bionetworks, Fred Hutchinson Cancer Research Center, Seattle, USA

[6]Department of Gastrointestinal Surgery, Oslo University Hospital, Oslo, Norway

[7]Institute for Clinical Medicine, University of Oslo, Oslo, Norway

*Shared first authorship

Running title: Drug responses among consensus molecular subtypes of CRC.

Key words: Colorectal cancer; consensus molecular subtypes; drug screening, HSP90 inhibitors; preclinical models.

Abbreviations list: 5-FU, 5-fluorouracil; CRC, colorectal cancer; CMS, consensus molecular subtypes; DSS, drug sensitivity score; EMT, epithelial to mesenchymal transition; FDR, false discovery rate; GEO, NCBI's Gene Expression Omnibus; HTA, Affymetrix Human Transcriptome 2.0 arrays; HR, hazard ratio; MSI, microsatellite instability; MSS, microsatellite stable; NTP, nearest template prediction; OS, overall survival; PCA, principal components analysis; PDX, patient-derived xenograft; RF, random forest; RFS, relapse-free survival; TCGA, The Cancer Genome Atlas.

Financial support: This study was supported by the Norwegian Cancer Society (project number 6824048-2016 to A. Sveen and project number 182759-2016 to R.A. Lothe), the Southern and Eastern Norway Regional Health Authority (to R.A. Lothe), the foundation *Stiftelsen Kristian Gerhard Jebsen* (to R.A. Lothe), the Research Council of Norway (*FRIPRO Toppforsk*, project number 250993; and grants to the Norwegian Cancer Genomics Consortium, both to R.A. Lothe), the European Union Seventh Framework Programme (FP7-PEOPLE-2013-COFUND, grant agreement number 609020 - *Scientia Fellows* to R.A. Lothe), and Merck KGaA, Darmstadt, Germany (Grant for Oncology Innovation 2015, "*Next generation of clinical trials with matched targeted therapies in colorectal cancer*" to R. Dienstmann and J. Guinney). Merck KGaA reviewed the manuscript for medical accuracy only before journal submission. The authors are fully responsible for the content of this manuscript, and the views and opinions described in the publication reflect solely those of the authors.

Corresponding author: Ragnhild A. Lothe, Department of Molecular Oncology, Institute for Cancer Research, Oslo University Hospital, P.O.Box 4953 Nydalen, NO-0424 Oslo, Norway; Phone: +47 22781728; Fax: +47 22781745; E-mail: rlothe@rr-research.no

Conflicts of interest: J. Tabernero has had Consultant/Advisory role for Amgen, Bayer, Boehringer Ingelheim, Celgene, Chugai, Genentech, Lilly, MSD, Merck Serono, Novartis, Roche, Sanofi, Symphogen, Taiho and Takeda. The other authors have no conflicts of interest.

Word count: 5,704

Total number of figures and tables: 6

Translational relevance

The number of stratified treatment options is limited in colorectal cancer, and there is great potential to improve treatment efficacy by molecularly-guided repurposing of targeted drugs. We translate consensus molecular subtyping (CMS) to preclinical models by development of a cancer cell-adapted CMS classifier, and combined with high-throughput drug sensitivity screening, we demonstrate that subtypes linked to poor prognosis in the metastatic setting (CMS1 and CMS4) have a strong relative sensitivity to HSP90 inhibition *in vitro*, and confirm that CMS2 is predictive of response to EGFR and HER2 inhibition. In a patient-derived xenograft (PDX) model of an aggressive and chemoresistant CMS4, combined administration of 5-fluorouracil and the HSP90 inhibitor luminespib showed a potential for improved treatment efficacy.

Abstract

Purpose: Response to standard oncological treatment is limited in colorectal cancer (CRC). The gene expression-based consensus molecular subtypes (CMS) provide a new paradigm for stratified treatment and drug repurposing, however, drug discovery is currently limited by the lack of translation of CMS to preclinical models. **Experimental Design:** We analyzed CMS in primary CRCs, cell lines and patient-derived xenografts (PDXs). For classification of preclinical models, we developed an optimized classifier enriched for cancer cell-intrinsic gene expression signals, and performed high-throughput *in vitro* drug screening (n=459 drugs) to analyze subtype-specific drug sensitivities. **Results:** The distinct molecular and clinicopathological characteristics of each CMS group were validated in a single-hospital series of 409 primary CRCs. The new, cancer cell-adapted classifier was found to perform well in primary tumors, and applied to a panel of 148 cell lines and 32 PDXs, these CRC models were shown to recapitulate the biology of the CMS groups. Drug screening of 33 cell lines demonstrated subtype-dependent response profiles, confirming strong response to EGFR and HER2 inhibitors in the CMS2 epithelial/canonical group, and revealing strong sensitivity to HSP90 inhibitors in cells with the CMS1 microsatellite instability/immune and CMS4 mesenchymal phenotypes. This association was validated *in vitro* in additional CMS-predicted cell lines. Combination treatment with 5-fluorouracil and luminespib showed potential to alleviate chemoresistance in a CMS4 PDX model, an effect not seen in a chemosensitive CMS2 PDX model. **Conclusions:** We provide translation of CMS classification to preclinical models and uncover a potential for targeted treatment repurposing in the chemoresistant CMS4 group.

Introduction

Colorectal cancer (CRC) is a worldwide health burden, representing the third most common type of cancer and the fourth most common cause of cancer deaths (1). Treatment decisions are primarily based on cancer stage and tumor location; however, clinical outcome varies greatly, both with respect to prognosis and treatment response (2). The repertoire of targeted treatments and the number of stratified treatment options based on prognostic and/or predictive factors is limited (3, 4). CRC is heterogeneous also at the molecular level (5, 6). This heterogeneity confers primary or secondary resistance to targeted treatments (7) and represents a major challenge for precise interpretation of prognostic and predictive markers (8).

Molecular classification of CRC has evolved in recent years. Until now, this has been based on the non-overlapping genomic phenotypes microsatellite instability (MSI) and chromosomal instability, providing both prognostic and predictive information. MSI+ tumors associate with good patient outcome in early stages (9), likely related to a large mutation burden (10, 11) and cytotoxic immune cell infiltration (12). In the metastatic setting, patients with MSI+ tumors have a poor prognosis (13), but respond well to immune checkpoint inhibition (14). The majority of CRCs have chromosomal instability, and aneuploidy is a predictor of a poor prognosis (15). Recently, more detailed classification of primary CRC has been proposed based on intrinsic gene expression profiles (16-20), resulting in the four biologically distinct consensus molecular subtypes (CMS) (21): CMS1 MSI-immune; CMS2 epithelial and canonical; CMS3 epithelial and metabolic; and CMS4 mesenchymal. The CMS classification has prognostic value independent of cancer stage, with dismal survival

outcomes for the CMS4 population, even when treated with standard adjuvant chemotherapies (22). A potential predictive value of the CMS groups has also been suggested from retrospective analysis of clinical trials, including lack of benefit from oxaliplatin (22) and anti-EGFR treatment (17, 23) in tumors with a mesenchymal-like phenotype, the latter independent of *RAS* mutation status. However, increased understanding of the unique drug sensitivities of the individual CMS groups has great potential to advance precision medicine in CRC.

Recognizing that the tumor microenvironment is an important contributor to gene expression signals in bulk tumor tissue (24-26), the translation of CMS classification to preclinical models, including cell lines and patient-derived xenografts (PDX) has major challenges. Although CMS labels have previously been assigned to CRC cell lines (27), development of "adapted" CMS classifiers carefully optimized for preclinical exploration is critical to investigate specific drug sensitivities of subtypes in high-throughput screens. Additionally, the question of whether these *in vitro* models precisely recapitulate the biology of CMS classification has not been resolved.

Here, we studied the distinct molecular and clinicopathological properties of CMS in an independent, single-hospital series of primary CRCs. Next, we developed a cancer cell-adapted CMS classifier for analysis of preclinical models, and performed high-throughput *in vitro* drug screening to identify subtype-specific drug sensitivities.

Methods

Patient material

A consecutive, population-based series of 409 patients treated surgically for stage I-IV CRC at Oslo University Hospital, Oslo, Norway, between 2005 and 2013 was included (Supplementary Table S1). The study was approved by the Regional Committee for Medical and Health Research Ethics, South Eastern Norway (REC number 1.2005.1629). All patients provided written informed consent, and the study was conducted in accordance with the Declaration of Helsinki. Details of DNA/RNA extraction, as well as MSI status and mutation analyses are included as Supplementary Text.

CRC cell lines

Totally 169 CRC cell lines were analyzed (Supplementary Table S2), including 38 cell lines in-house (details of growth conditions in Supplementary Text) and publicly available gene expression data from 136 cell lines (five overlapping with the in-house dataset; obtained from Gene Expression Omnibus [GEO] accession numbers GSE36133 (28), GSE57083 and GSE59857 (29)). The number of cell lines derived from unique patients was 148. Cell line identities were verified by fingerprinting according to the AmpFLSTR Identifiler PCR Amplification Kit (Life Technologies by Thermo Fisher Scientific), and matched to the profiles reported by the American Type Culture Collection. Cell lines were regularly tested for mycoplasma contamination according to the MycoAlert Mycoplasma Detection Assay (Lonza Walkersville Inc., Walkersville, MD, USA).

Gene expression analysis

The primary CRCs were analyzed for gene expression using Affymetrix GeneChip Human Exon 1.0 ST Arrays (HuEx; n = 201 CRCs) or Human Transcriptome 2.0 Arrays (HTA; n = 208 CRCs) according to the manufacturer's instructions (Affymetrix Inc., Santa Clara, CA, USA). The in-house cell lines were analyzed on HTA arrays. The data have partly been published previously (GEO accession numbers GSE24550, GSE29638, GSE69182, GSE79959, and GSE97023) and the remaining samples (n = 174 CRCs) have been deposited to GEO with accession number GSE96528. Details of data pre-processing of the in-house and public datasets, as well as CMS classification of the primary CRCs are included as Supplementary Text. Gene set expression enrichment analyses were performed using the R package GSA (30) and a customized collection of 51 CRC-related gene sets. Sample-wise gene set expression enrichment scores were calculated using the R package GSVA (31).

Development of the cancer cell-adapted CMS classifier

A CMS classifier enriched for cancer cell-intrinsic gene expression signals was developed based on RNA sequencing data from primary CRCs in The Cancer Genome Atlas (TCGA; n = 560) and CRC cell lines (n = 37 unique) (32), as well as a public microarray dataset of PDX tumors and primary CRCs (n = 40 and 30, respectively) (33). For the TCGA data, preprocessed gene-level RSEM expression values were downloaded from the Broad GDAC Firehouse (level 3; doi:10.7908/C11G0KM9) and CMS assignments from the Colorectal Cancer Subtyping Consortium web site at SAGE Synapse (21). The samples were randomly assigned to a training (75%, n = 417) and a test (25%, n = 143) dataset.

Genes with subtype-specific expression were identified as genes with high relative expression in each CMS group in the TCGA training set. Differential expression analysis was done by comparing each subtype with the rest using the voom approach with quantile normalization in the R package limma, and genes with a $\log_2$ fold-change > 1 and adjusted P-value < 0.1 in each subtype were retained. To enrich for genes likely to be informative in cell lines and PDX models, and to exclude genes with high expression in the tumor microenvironment, two additional filters were applied. First, only genes with high expression in CRC cell lines (top 25% expressed genes in at least three samples) and high expression variation (top 25% inter-percentile range [10^{th} to 90^{th}] among the samples) in the RNA sequencing cell line dataset were retained. Second, genes with high expression in primary CRCs compared to PDX tumors were filtered out, retaining only genes with a mean $\log_2$ fold-change below 2 in the primary CRC *versus* PDX dataset.

Based on this filtered template gene set representing cancer cell-adapted expression signatures of each CMS group, a collection of 148 CRC cell lines derived from unique patients (totally 169 cell lines) was classified using the Nearest Template Prediction (NTP) algorithm (34) with cosine correlation distances to predict the proximity of each sample to the four template signatures. P-values and false discovery rates (FDRs) were calculated based on random resampling (n = 1,000) of the template genes. Sensitivity analysis of the gene expression thresholds applied during filtering of the template gene set is described in the Supplementary Text.

CMS classification of PDX models

PDX models of primary CRCs or liver metastases (n = 32) were established as previously described (35). One tumor from each mouse and samples from four matching primary CRCs were analyzed for gene expression on Affymetrix Human Gene 2.0 ST arrays (details of data pre-processing in the Supplementary Text). Sample classification was performed using the adapted CMS classifier.

Drug screening in CRC cell lines

An in-house collection of 33 cell lines (Supplementary Table S2b) was analyzed for drug sensitivities in an *in vitro* screen using an established high-throughput platform (36) including 459 clinically approved or investigational drugs representing different molecular target classes. A drug sensitivity score (DSS) (37) was calculated per drug and cell line relative to a negative and a positive control, based on cell viability after drug treatment at five different concentrations over a 10,000 fold concentration range. Drugs (n = 218) with low efficacy (DSS values above 7 in less than three cell lines) and low variation in DSS values (cross-sample range below 7) were excluded from further analyses. Differential drug sensitivity among sample groups was analyzed by independent samples t-tests.

Transcriptional profiling and western blotting in cells treated with luminespib

Three CMS4 cell lines with varying levels of sensitivity to HSP90 inhibition (CACO2, LIM2099 and SW480) were seeded in 60 mm dishes 24 hours prior to exposure to DMSO (control) or 50 nM luminespib. RNA was isolated after treatment for 6 hours (Qiagen Allprep

DNA/RNA/miRNA Universal kit) and analyzed on Affymetrix HTA microarrays. Differential gene expression analysis was performed by paired samples t-tests comparing treated and control cells using limma. Protein expression of HSP70 and HSP40 was analyzed by western blotting (Supplementary Text).

Animals, xenotransplantation and treatments

Among the 32 PDX models classified according to CMS, one model characteristic of CMS4 (patient ID 43) and one of CMS2 (patient ID 1) were selected for drug treatment. Experiments were conducted following the European Union's animal care directive (2010/63/EU) and were approved by the Ethical Committee of Animal Experimentation of VHIR (Vall d'Hebron Institute of Research)/VHIO (Vall d'Hebron Institute of Oncology; ID: 18/15 CEEA). NOD-SCID (NOD.CB17-*Prkdc*^{scid}/NcrCrl) mice were purchased from Charles River Laboratories (Wilmington, MA, USA). One hundred thousand patient-derived cells suspended in PBS were mixed with Matrigel (1:1 v/v-ratio; BD Biosciences, San Jose, CA, USA) and injected subcutaneously into both flanks of NOD-SCID mice. When the tumor reached 0.5 cm^3 in volume, mice (n = 34 for both models) were randomized to each of four different treatment arms, including a control arm (empty vehicle), 5-fluorouracil (5-FU) monotherapy, luminespib (HSP90 inihibitor) monotherapy, and 5-FU + luminespib combination therapy. Luminespib (25 mg/kg in PBS, MCE, Monmouth Junction, NJ, USA) was administered by intraperitoneal injection three times per week. 5-FU (40mg/kg in PBS; Sigma-Aldrich, St. Louis, MO, USA) was administered by intraperitoneal injection twice per week. When matching end-point criteria, mice were euthanized and complete necropsies

were performed. Protein expression of HSP70 and Ki67 was analyzed in post-treatment tissue samples by immunohistochemistry (Supplementary Text).

Statistical analyses

Statistical tests were conducted in R (v.3.3.3), including Fisher's exact test of contingency tables with the function fisher.test, t-tests with equal or unequal variances (Welch's t-test) using the function t.test, prediction accuracy using the confusionMatrix-function in the package caret, and two one-sided test for equivalence using the tost-function in the package equivalence, with the magnitude of similarity determined by the parameter epsilon. Unsupervised principal components analysis (PCA) was done using the prComp function. Univariable and multivariable survival analyses were conducted with Cox's proportional hazards regression, with calculation of P-values from Wald's tests for predictive potential using the SPSS software version 21 (IBM Corporation, Armonk, NY, USA). Kaplan-Meier survival curves were compared with the log-rank test. Five-year relapse-free survival (RFS, considering relapse after complete resection or death from any cause as events) and overall survival (OS, considering death from any cause as events) were used as endpoints. Anti-tumor activity in PDX models was analyzed using a generalized linear mixed model of tumor volume fold changes, with random effects and treatment arm and time as covariates.

Results

Validation of clinicopathological and biological associations of CMS in primary CRC

A prospective, single-hospital series of primary CRCs (n = 409; Supplementary Table S1) was classified according to CMS based on gene expression profiles using the random forest (RF) predictor implemented in the R package CMSclassifier (21) (Fig. 1a). The previously described molecular (MSI status, *BRAF*, *KRAS* and *TP53* mutations) and clinicopathological (patient gender, tumor localization, tumor differentiation grade and cancer stage) associations of each subtype were confirmed (Fig. 1b-c; Supplementary Tables S3 and S4; Supplementary Text). In particular, patients with CMS4 tumors had a poorer 5-year RFS and OS rate than patients with CMS1-3 tumors (hazard ratio [HR] = 1.8 [95% confidence interval, CI, 1.2-2.7] and 2.0 [95% CI 1.3-3.1]; P = and 0.005 and 0.001 for RFS and OS, respectively; see also Fig. 1d and Supplementary Fig. S1a). This was independent of known clinicopathological prognostic factors and MSI status in multivariable analyses (HR = 1.4 [95% CI 0.9-2.2] and 1.6 [95% CI 1.04-2.6], P = 0.1 and 0.03 for 5-year RFS and OS, respectively; Supplementary Table S5). The distinct biological properties of each CMS group, including infiltration patterns of immune and stromal cells, were also validated by gene set expression enrichment analyses (Fig. 1e, Supplementary Fig. S1b, Supplementary Table S6 and Supplementary Text).

CMS classification of preclinical models

Our main interest was to study CMS-specific drug sensitivities in cell line models and particularly in the poor prognostic CMS4 group. As confirmed in our clinical cohort, the transcriptome of CMS4 primary CRCs is greatly influenced by signals from the tumor microenvironment, and application of the original RF CMSclassifier to a collection of 148 unique CRC cell lines showed that it failed to accurately identify this subtype in the *in vitro*

models. Using default settings, 82 cell lines (55%) were unclassified and among the classified, 41 (62%) were CMS2 and only 3 (5%) were CMS4 (Supplementary Fig. S2a). Gene set analyses showed that the 3 CMS4 cell lines indeed had clear CMS4 characteristics, including epithelial to mesenchymal transition (EMT) and TGFβ responses, but this was true also for additional, unclassified samples (Supplementary Fig. S2b). Furthermore, this classification failed to accurately distinguish between the two epithelial subtypes CMS2-canonical and CMS3-metabolic (Supplementary Fig. S2c). To improve the classification of preclinical models, we therefore generated a novel CMS classifier enriched for cancer cell-intrinsic gene expression signals (Fig. 2a; details of the public expression datasets and analysis thresholds used are included in the Methods). First, potential template genes were identified as genes with high relative expression in each CMS group in primary CRCs (n = 1,994 unique genes; Supplementary Table S7). Next, this gene set was filtered to exclude (i) genes with a low expression level or expression variation in CRC cell lines (n = 1,454 genes) and (ii) genes expressed in the tumor microenvironment, identified as genes with a high expression in primary CRCs compared to PDX tumors (n = 57 additional genes; Supplementary Table S7). The resulting list of genes (n = 483; Supplementary Table S8) were used as templates for CMS classification based on the NTP algorithm (34). This new classifier is publicly available as the R package CMScaller and can be downloaded from https://github.com/Lothelab/CMScaller (Eide *et al*., submitted).

To assess prediction accuracy in patient samples, the adapted CMS classifier was applied to four independent series of primary CRCs (total n = 709) analyzed on four different gene expression platforms. Classification concordance compared with the original RF

CMSclassifier ranged from 85% to 92%, demonstrating robust performance independent of analysis platform (Table 1).

CRC cell lines

CMS classification was obtained for 126 (85%) of the 148 unique CRC cell lines using the adapted classifier and an FDR threshold from NTP of 0.2 (Supplementary Table S2a). The CMS distribution across the cell lines was similar to the in-house patient series (Fig. 2b; $P < 0.05$ from paired test of equivalence with magnitude of similarity above 8). In comparison with the original RF CMSclassifier, the concordance in subtype assignments for cell lines classified by both approaches was high (88%), and the added value of the adapted classifier was primarily the higher classification rate, in particular in CMS3 and CMS4 (Supplementary Table S9). To determine whether key characteristics of the CMS groups were recapitulated in the cell lines, we explored associations between CMS and other molecular data. Similarly to primary CRCs, CMS1 cell lines showed strong enrichment for MSI ($P = 2\times10^{-4}$) and *BRAF* mutations ($P = 6\times10^{-4}$; Fig. 2c and Supplementary Table S10). CMS3 cell lines were frequently MSI+ and *KRAS* mutated, while *TP53* mutations were enriched in CMS2, although not statistically significant. Gene expression-based PCA indicated that CMS1/4 *versus* CMS2/3 represented the primary sample split ($P = 2\times10^{-28}$ from comparison of principal component 1 (PC1) between the two sample groups; Supplementary Fig. S3), and gene set analyses confirmed that CMS1 and CMS4 cell lines were undifferentiated, while CMS2 and CMS3 showed clear epithelial characteristics (Fig. 2d and Supplementary Table S11). CMS2 and CMS3 additionally had up-regulation of HNF4A targets, while CMS3 was

particularly enriched for metabolic pathways. CMS4 was specifically characterized by EMT activation, extracellular matrix organization and TGFβ responses.

Optimal performance of the classifier is dependent on unbiased representation of all CMS groups in the query sample set, and to estimate stability, cell line classification was repeated after random resampling of cell line subsets (n = 1,000 resamplings of 50% of the cell lines). The majority of cell lines (82% of the 148 unique) retained their CMS group in more than 95% of the resamplings (Supplementary Table S12). The classification uncertainty was highest in CMS1 (Supplementary Fig. S4a), which may be associated with an enrichment of MSI+ samples in the cell line collection (38% *versus* 18% in our patient series). However, gene set expression analysis specifically among MSI+ cell lines showed expected CMS-associations, also for CMS1 (Supplementary Fig. S4b).

To assess the independence of the adapted classifier from tumor stroma, the stromal and epithelial compartments of laser microdissected primary CRCs (GSE35602) (38) were analyzed. Some template genes had high relative expression in the stromal samples (Supplementary Fig. S5), and an additional template gene filter was therefore tested by excluding these genes (Supplementary Table S7). Cell line classification with the reduced template gene set was highly concordant with the initial adapted classifier (90% accuracy [95% CI 83%-95%] among the confidently classified cell lines; Supplementary Table S12), indicating that the influence of stromal gene expression signals on sample classification was low. Furthermore, gene set analyses and resampling of the cell lines (as above) indicated that

the reduced template gene set did not improve the subtype assignment or classification stability (Supplementary Fig. S5).

Patient-derived xenografts

The adapted classifier was also applied to a set of 32 PDX models of CRC (22 derived from primary tumors and 10 from liver metastases), and the matching primary tumor from four patients. Subtype assignment was obtained for 28 (88%) of the PDX tumors (FDR from NTP lower than 0.2), including 7 (25%) to CMS1, 13 (46%) to CMS2, 5 (18%) to CMS3, and 3 (11%) to CMS4. Concordant subtypes were assigned for three of the four matching PDX-patient tumor pairs (Supplementary Table S13). Although with a lower sample number, the *in vivo* models also recapitulated important features of the CMS groups. In concordance with results from the patient series and cell lines, CMS1/4 *versus* CMS2/3 represented the primary sample split based on gene expression PCA (Supplementary Fig. S6). Furthermore, gene set expression analyses showed that CMS1 was enriched for "MSI-like" and "*BRAF*-mutant-like" PDX tumors, while CMS2 and CMS3 had epithelial characteristics, with enrichment of colonic differentiation signatures. CMS2 additionally had high WNT signaling and CMS3 had enrichment of metabolic signatures. CMS4 showed enrichment for angiogenesis. For comparison, PDX classification based on the reduced template gene set (additionally filtered for stromal gene expression) was highly concordant (93% accuracy [95% CI 77%-99%]).

CMS defines subgroups of cell lines with distinct drug response profiles

To explore subtype-specific drug responses, 33 cell lines established from 29 patients (Supplementary Table S2b) were selected for *in vitro* pharmacogenomic profiling using an established high-throughput drug screening platform (n = 459 drugs; Supplementary Table S14) (36). Drug sensitivity scores (DSS) (37) were calculated for each drug based on cell viability after treatment at five different concentrations, and quality control showed strong reproducibility of the DSS values between independent drug screens of the same cell line (RKO; Pearson correlation 0.99, standard deviation of difference between repeated screens 1.36). Furthermore, drug screen reproducibility between paired cell lines from each of four patients was associated with their pair-wise similarity in gene expression (Supplementary Fig. S7a). For subgroup comparisons, paired cell lines were excluded (HCT15, WIDR, SW620, and IS1), and the final set (n = 29) represented all four CMS groups (n = 7, 9, 5 and 8 predicted CMS1, 2, 3 and 4, respectively, not restricted by the FDR from CMS prediction; Supplementary Fig. S7b).

Principal component analysis based on DSS values from the drug screen indicated a separation of the cell lines into two response groups by MSI status (Supplementary Fig. S8a; $P = 7\times10^{-7}$ by Welch's t-test comparing PC1 between MSI+ and microsatellite stable, MSS, samples). Comparisons of individual drug responses between the two sample groups confirmed that this distinction was primarily caused by a strong relative sensitivity to chemotherapeutic drugs in MSI+ cell lines, in particular topoisomerase inhibitors and gemcitabine (Supplementary Fig. S8b and Supplementary Table S15). CMS accounted for additional variation in DSS values (Supplementary Fig. S8c) and to explore subtype-specific sensitivities, drug response comparisons were made between all the individual CMS groups

(Fig. 3 and Supplementary Table S16). Consistent with the high prevalence of MSI in CMS1, CMS1 cell lines were more sensitive to anti-metabolites and inhibitors of topoisomerases and mitosis than CMS2. Additionally, CMS1 showed stronger sensitivity to heat shock protein 90 (HSP90) inhibitors than both CMS2 and CMS3. There were few drugs with differential sensitivity between CMS1 and CMS4, or between CMS2 and CMS3. However, CMS2 cell lines were more sensitive to EGFR and HER2 inhibitors than both CMS3 and CMS4. CMS4 cell lines showed strong sensitivity to HSP90 inhibitors, atorvastatin (HMG-CoA reductase inhibitor), 2-methoxyestradiol (2ME; combined angiogenesis and tubulin inhibitor) and disulfiram (inhibitor of alcohol dehydrogenase) compared to both CMS2 and CMS3 (these selected drug screen data are available in Supplementary Table S17).

Summarized, these comparisons indicated that EGFR and HER2 inhibitors had particularly strong activity in CMS2, which was confirmed in a direct comparison of CMS2 *versus* CMS1/3/4 cell lines (Fig. 4a and Supplementary Table S18). Strong relative response to anti-EGFR treatment in CMS2 was also validated in published data of cetuximab treatment in 130 unique cell lines (29), independent of *KRAS* and *BRAF* mutation status (Supplementary Fig. S9). Additionally, CMS1 and CMS4 appeared to be sensitive to similar classes of agents, in line with the major distinction observed in the gene expression data between the undifferentiated CMS1/4 and epithelial-like CMS2/3 cell lines. Indeed, correlation analyses between PC1 of the DSS values and sample-wise gene set expression enrichment scores (calculated using the R package GSVA (31); gene sets listed in Supplementary Table S6), showed that the overall drug response pattern among the cell lines was most strongly correlated to a colonic differentiation signature ("colonic crypt, top"; Spearman correlation -

0.7, P = 2×10^{-5}; Supplementary Fig. S8d). Accordingly, CMS1/4 cell lines were compared to CMS2/3, and a strong relative response to several HSP90 inhibitors (luminespib, ganetespib and radicicol), 2ME, indibulin (another tubulin-inhibitor), atorvastatin, and tipifarnib (farnesyltransferase inhibitor) in CMS1/4 was confirmed (Fig. 4b and Table 2). These same drugs had stronger relative activity in CMS1/4 also when analyzing MSS cell lines only, when including only cell lines with FDR from CMS assignment below 0.2, when including the opposite set of the paired cell lines, and based on CMS classification using the reduced template gene set (additionally filtered for stromal gene expression; Supplementary Fig. S10).

Strong relative activity of HSP90 inhibitors in CMS1 and CMS4 is validated *in vitro*

For independent biological validation of differential drug activity in CMS1/4 compared to CMS2/3 cell lines, five additional cell lines were predicted to belong to either the CMS1 (LIM2405) or CMS4 (CAR1, HCA7, LIM2099 and OUMS23) subtypes based on their gene expression profiles, and subsequently screened for drug sensitivities with the same experimental setup as in the initial discovery screen. Two CMS3 cell lines (HT29 and LS174T) were included as controls in the validation drug screen. Clear differential sensitivity for all three HSP90 inhibitors (luminespib, ganetespib and radicicol), 2ME, atorvastatin and disulfiram was validated in CMS1 and CMS4 compared to CMS3 (Fig. 4c).

Furthermore, strong sensitivity to HSP90 inhibition in CMS1 and CMS4 was validated in public drug response data from 15 CRC cell lines (9 overlapping with our drug screen) treated with ganetespib (39). The cell lines were classified using the adapted classifier and the

CMS1/4 group was found to have lower IC_{50}-values for ganetespib (mean 24 nM) than CMS2/3 (mean 52 nM), indicating higher sensitivity in the first group (Supplementary Fig. S11a). Similarly, among 32 CRC cell lines from the Genomics of Drug Sensitivity in Cancer Project (16 overlapping with our drug screen), higher sensitivity to the HSP90 inhibitor CCT018159 was confirmed in CMS1/4 (average $\log_e(IC_{50}$ in µM) 3.4) compared to CMS2/3 (average $\log_e(IC_{50}$ in µM) 5.6, P = 0.0004 by Welch's t-test). Here, stronger relative sensitivity in CMS1/4 was found also among MSS cell lines only (Supplementary Fig. S11b).

HSP90 inhibition is associated with up-regulation of heat shock response

To identify the transcriptional changes associated with response to HSP90 inhibition, three CMS4 cell lines (CACO2, LIM2099 and SW480) were treated with luminespib. Differential gene expression analysis of treated compared to control cells (DMSO) showed that up-regulation of heat shock response was the dominant response mechanism, with up-regulation of several members of the HSP family (Fig. 4d and Supplementary Table S19). Up-regulation of two main HSP90 co-chaperones, HSP70 and HSP40, was confirmed at the protein level (Supplementary Fig. S12a). Heat shock transcription factor 1 (HSF1) and its transcriptional activity has previously been described to be a resistance mechanism against HSP90 inhibition, and concordantly, PCA revealed significant dysregulation of a previously published gene expression signature of HSF1 (40) in treated *versus* control cells (P = 0.03 from paired t-test of PC1; Supplementary Fig. S12b). Among the 29 cell lines in the initial drug screen panel, PC1 of the HSF1 signature was strongly correlated to the DSS values of all three HSP90 inhibitors and was also significantly different between CMS1/4 and CMS2/3 (Supplementary Fig. S12c).

HSP90 inhibition may alleviate chemoresistance in CMS4 *in vivo*

In our drug screen panel, CMS4 had a particularly poor response to fluoropyrimidines ($P \leq 0.05$ among MSS cell lines; Supplementary Fig. S13). Previous studies have suggested that HSP90 inhibition may sensitize CRC cell lines to chemotherapy, and although monotherapy with HSP90 inhibitors has shown low efficacy in metastatic CRC (42), response has been obtained by combination therapy with HSP90 inhibitors and capecitabine (5-FU pro-drug) in patients who have progressed on fluoropyrimidines (43). Accordingly, to analyze a potential effect of HSP90 inhibition *in vivo*, we selected a CMS4 PDX model (MSS, *KRAS*/*NRAS* wild type, $BRAF^{V600E}$ mutated) for treatment in a randomized and controlled set-up. Immunodeficient NOD-SCID mice (n = 34) were injected with cells derived from a liver metastasis of a chemotherapy-naïve CRC patient and randomized to four treatment arms: (i) control arm with vehicle; (ii) single agent 5-FU; (iii) single agent luminespib; and (iv) combination therapy with 5-FU + luminespib. Consistent with the cell line data, this CMS4 model showed poor response to chemotherapy (Fig. 4e). Chemoresistance was confirmed by staining for the proliferation marker Ki67 in post-treatment samples, and there were no significant changes in Ki67 expression in mice receiving 5-FU compared to vehicle-treated controls. Furthermore, monotherapy with luminespib did not impact on tumor growth, but combined administration of 5-FU + luminespib resulted in significantly greater anti-tumor activity compared to vehicle-treated control (50% reduction in tumor growth, $P < 0.001$ in generalized linear model) and 5-FU single agent (33% reduction in tumor growth, $P < 0.001$). Significant up-regulation of HSP70 after treatment with luminespib (both as monotherapy and combined with 5-FU) indicated a specific pharmacodynamic effect of HSP90 inhibition and therefore target dependency. The combination of fluoropyrimidines with HSP90

inhibition was well tolerated, on the basis of minimal changes in mouse body weight. For control, a CMS2 PDX model (MSS, *KRAS*/*NRAS*/*BRAF* wild type, *TP53* mutated) was treated with the same experimental setup. Inconsistent with the cell line data, single-agent luminespib had a stronger effect on tumor growth in this model, however, HSP90 inhibition (monotherapy or in combination with 5-FU) was not associated with increased expression of HSP70 in post-treatment samples, suggesting that the inhibitory activity was likely a result of off-target effects (Fig. 4f). Furthermore, this model was highly chemosensitive, as shown by a strong reduction in tumor growth and reduced proliferation in post-treatment samples (Ki67 expression) after treatment with 5-FU compared to vehicle-treated controls, and no synergistic effect of combination treatment with luminespib was detected at the end of the experiment.

Discussion

Response to standard oncological treatment is limited in CRC and there is great potential to improve treatment efficacy by molecularly-guided repurposing of targeted drugs. We identify strong relative activity of HSP90 inhibitors in *in vitro* models of the transcriptomic CMS1 and CMS4 groups of CRC by high-throughput drug screening, using a new and cancer cell-adapted CMS classifier. HSP90 inhibition has previously been extensively investigated in cancer and has demonstrated anti-tumor activity in several solid tumor types, mainly as combination therapies (41). However, low response rates are observed in unstratified patient populations. In the only phase II trial reported in CRC, single-agent treatment with ganetespib demonstrated good tolerance but low efficacy in chemotherapy-refractory metastatic disease, independent of *KRAS* mutation status (42). Higher anti-tumor activity was

seen in early clinical trials exploring combinations of HSP90 inhibitors with chemotherapies, including fluoropyrimidines (5-FU and capecitabine) (43). Our study confirms stronger *in vivo* anti-tumor activity of combination therapy with HSP90 inhibitors and 5-FU in a chemoresistant CMS4 PDX model. This is concordant with published *in vitro* data showing that HSP90 inhibition sensitizes CRC cell lines to the effect of 5-FU, oxaliplatin and topoisomerase inhibitors (39, 44, 45). Specifically, our PDX results are in line with a CMS4 cell line-derived xenograft (HCT116) experiment, where ganetespib significantly potentiated the anti-tumor efficacy of capecitabine, causing tumor regression in a model that is intrinsically resistant to fluoropyrimidine therapy. No synergy between chemotherapy and HSP90 inhibition was observed in the CMS2 model, but this model was highly chemosensitive and in contrast to CMS4 also showed response to single-agent luminespib, although likely as an off-target effect. Accordingly, these experiments do not allow us to make a conclusive statement on a CMS-dependent effect of HSP90 inhibition *in vivo*. However, reduced benefit from chemotherapy has been documented in patients harboring a mesenchymal-like phenotype (19, 22), and consistently, both the CMS4 cell lines and our CMS4 PDX model showed poor relative response to fluoropyrimidines. Efficient tumor shrinkage is difficult to achieve in mouse models of this aggressive subtype, and addition of luminespib showed potential to alleviate chemoresistance, although with a moderate anti-tumor effect. The failure to achieve complete remission raises the questions whether tumor-stroma interactions may modify the drug response *in vivo* and whether the optimal partners for HSP90 inhibitors in CMS4 are drugs targeting stromal dependencies. Larger *in vivo* studies with additional models are needed prior to clinical translation. However, the encouraging preclinical data presented here suggest that targeted inhibitors can overcome chemoresistance in selected CRC populations, opening the door for future investigations.

Mechanistically, we still need to study the intrinsic cancer cell biological determinants of HSP90 inhibitor sensitivity in CRC. HSP90 is a molecular chaperone that maintains the homeostasis of many different client proteins and consequently, HSP90 inhibition may block multiple oncogenic signaling pathways simultaneously (39, 44). Several potential mechanisms of resistance have been described, including compensatory up-regulation of heat shock response by the transcription factor HSF1, involving particularly the pro-survival chaperones HSP70 and HSP27 (46). We confirm transcriptional up-regulation of heat shock response in CMS4 cell lines after HSP90 inhibition, indicating a specific response to the targeted treatment. Up-regulation of HSP70 in CMS4 PDX models treated with luminespib confirmed target engagement also *in vivo* in this subtype.

The original CMS classifier is appropriate only for fresh frozen samples from primary CRCs, and development of a more generally applicable classifier is paramount for clinical translation. To this end, we have developed a cancer cell-adapted CMS classifier and provide CMS classification of a set of 148 widely used CRC cell lines. In CRC in particular, cell lines have repeatedly been shown to represent the molecular properties of tumors (28, 29, 47-49) and we show that this is the case also for CMS classification. Although devoid of tumor stroma, the cell lines recapitulated the individual CMS groups and their biological properties. The adapted classifier is enriched for cancer cell-intrinsic gene expression signals, although not completely independent of the tumor microenvironment. Still, additional filtering of the template gene set to further reduce the potential influence of stromal gene expression had little impact on sample classification, indicating robustness. Importantly, the classifier

performed well also in tumor samples, confirming reproducibility of the classification in primary CRCs, and showing translation of the classification to PDX models, where contamination of gene expression signals from murine stroma may be a challenge. It has recently been recognized also by others that the original CMS classifier fails to identify some of the CMS groups not only in cell lines, but also in patient-derived organoids and xenografts (50). We argue that this may be alleviated by our adapted classifier.

Important features such as the level of intra- and/or inter-tumor heterogeneity of CMS, as well as the stability of the subtypes during metastatic progression, are still unknown. However, we validated the clinicopathological and biological properties of the CMS groups in a single-hospital series of primary CRCs. We also identified strong relative response to EGFR and HER2 inhibitors in cell lines of the CMS2 subtype. This is consistent with the high relative frequency of *EGFR* and *ERBB2* (encoding the HER2 protein) amplification in CMS2 (21), and with the strong sensitivity to cetuximab demonstrated in cell lines of the late transit-amplifying gene expression-based subtype (29) and in PDXs of a subtype with high WNT signaling (50), both of which are largely overlapping with CMS2. Altogether, this reinforces the potential of CMS as a framework for stratified treatment in CRC.

In conclusion, we show reproducibility of the CMS groups in primary CRC and provide translation of the classification to preclinical models. Drug screening of cell lines identified CMS1 and CMS4 as potential predictive biomarkers for response to HSP90 inhibition. *In vivo*, this targeted treatment may alleviate chemoresistance in CMS4. The poor patient

prognosis associated with CMS4 warrants additional studies to pursue the potential for clinical testing of HSP90 inhibitor repositioning and combination therapy in CRC.

References

1. Ferlay J, Soerjomataram I, Dikshit R, Eser S, Mathers C, Rebelo M, *et al*. Cancer incidence and mortality worldwide: sources, methods and major patterns in GLOBOCAN 2012. *Int J Cancer* **2015**;136:E359-86.
2. Linnekamp JF, Wang X, Medema JP, Vermeulen L. Colorectal cancer heterogeneity and targeted therapy: a case for molecular disease subtypes. *Cancer Res* **2015**;75:245-9.
3. Dienstmann R, Salazar R, Tabernero J. Personalizing colon cancer adjuvant therapy: selecting optimal treatments for individual patients. *J Clin Oncol* **2015**;33:1787-96.
4. Dienstmann R, Vermeulen L, Guinney J, Kopetz S, Tejpar S, Tabernero J. Consensus molecular subtypes and the evolution of precision medicine in colorectal cancer. *Nat Rev Cancer* **2017**;17:79-92.
5. Sottoriva A, Kang H, Ma Z, Graham TA, Salomon MP, Zhao J, *et al*. A Big Bang model of human colorectal tumor growth. *Nat Genet* **2015**;47:209-16.
6. Sveen A, Løes IM, Alagaratnam S, Nilsen G, Høland M, Lingjærde OC, *et al*. Intra-patient inter-metastatic genetic heterogeneity in colorectal cancer as a key determinant of survival after curative liver resection. *PLoS Genet* **2016**;12:e1006225.
7. Misale S, Di NF, Sartore-Bianchi A, Siena S, Bardelli A. Resistance to anti-EGFR therapy in colorectal cancer: from heterogeneity to convergent evolution. *Cancer Discov* **2014**;4:1269-80.

8. Perez K, Walsh R, Brilliant K, Noble L, Yakirevich E, Breese V, *et al*. Heterogeneity of colorectal cancer (CRC) in reference to KRAS proto-oncogene utilizing WAVE technology. *Exp Mol Pathol* **2013**;95:74-82.

9. Popat S, Hubner R, Houlston RS. Systematic review of microsatellite instability and colorectal cancer prognosis. *J Clin Oncol* **2005**;23:609-18.

10. The Cancer Genome Atlas Network. Comprehensive molecular characterization of human colon and rectal cancer. *Nature* **2012**;487:330-7.

11. Vogelstein B, Papadopoulos N, Velculescu VE, Zhou S, Diaz LA, Kinzler KW. Cancer genome landscapes. *Science* **2013**;339:1546-58.

12. Mlecnik B, Bindea G, Angell HK, Maby P, Angelova M, Tougeron D, *et al*. Integrative analyses of colorectal cancer show immunoscore is a stronger predictor of patient survival than microsatellite instability. *Immunity* **2016**;44:698-711.

13. Kim CG, Ahn JB, Jung M, Beom SH, Kim C, Kim JH, *et al*. Effects of microsatellite instability on recurrence patterns and outcomes in colorectal cancers. *Br J Cancer* **2016**;115:25-33.

14. Le DT, Uram JN, Wang H, Bartlett BR, Kemberling H, Eyring AD, *et al*. PD-1 blockade in tumors with mismatch-repair deficiency. *N Engl J Med* **2015**;372:2509-20.

15. Danielsen HE, Pradhan M, Novelli M. Revisiting tumour aneuploidy - the place of ploidy assessment in the molecular era. *Nat Rev Clin Oncol* **2016**;13:291-304.

16. Budinska E, Popovici V, Tejpar S, D'Ario G, Lapique N, Sikora KO, *et al*. Gene expression patterns unveil a new level of molecular heterogeneity in colorectal cancer. *J Pathol* **2013**;231:63-76.

17. De Sousa EM, Wang X, Jansen M, Fessler E, Trinh A, de Rooij LP, *et al*. Poor-prognosis colon cancer is defined by a molecularly distinct subtype and develops from serrated precursor lesions. *Nat Med* **2013**;19:614-8.

18. Marisa L, de Reynies A, Duval A, Selves J, Gaub MP, Vescovo L, *et al*. Gene expression classification of colon cancer into molecular subtypes: characterization, validation, and prognostic value. *PLoS Med* **2013**;10:e1001453.

19. Roepman P, Schlicker A, Tabernero J, Majewski I, Tian S, Moreno V, *et al*. Colorectal cancer intrinsic subtypes predict chemotherapy benefit, deficient mismatch repair and epithelial-to-mesenchymal transition. *Int J Cancer* **2014**;134:552-62.

20. Sadanandam A, Lyssiotis CA, Homicsko K, Collisson EA, Gibb WJ, Wullschleger S, *et al*. A colorectal cancer classification system that associates cellular phenotype and responses to therapy. *Nat Med* **2013**;19:619-25.

21. Guinney J, Dienstmann R, Wang X, de Reynies A, Schlicker A, Soneson C, *et al*. The consensus molecular subtypes of colorectal cancer. *Nat Med* **2015**;21:1350-6.

22. Song N, Pogue-Geile KL, Gavin PG, Yothers G, Kim SR, Johnson NL, *et al*. Clinical outcome from oxaliplatin treatment in stage II/III colon cancer according to intrinsic subtypes: secondary analysis of NSABP C-07/NRG Oncology randomized clinical trial. *JAMA Oncol* **2016**;2:1162-9.

23. Trinh A, Trumpi K, de Sousa EMF, Wang X, de Jong JH, Fessler E, *et al*. Practical and robust identification of molecular subtypes in colorectal cancer by immunohistochemistry. *Clin Cancer Res* **2016**;23:387-98.

24. Calon A, Lonardo E, Berenguer-Llergo A, Espinet E, Hernando-Momblona X, Iglesias M, *et al*. Stromal gene expression defines poor-prognosis subtypes in colorectal cancer. *Nat Genet* **2015**;47:320-9.

25. Isella C, Terrasi A, Bellomo SE, Petti C, Galatola G, Muratore A, *et al*. Stromal contribution to the colorectal cancer transcriptome. *Nat Genet* **2015**;47:312-9.

26. Becht E, de Reynies A, Giraldo NA, Pilati C, Buttard B, Lacroix L, *et al*. Immune and stromal classification of colorectal cancer is associated with molecular subtypes and relevant for precision immunotherapy. *Clin Cancer Res* **2016**;22:4057-66.

27. Fessler E, Jansen M, De Sousa EMF, Zhao L, Prasetyanti PR, Rodermond H, *et al*. A multidimensional network approach reveals microRNAs as determinants of the mesenchymal colorectal cancer subtype. *Oncogene* **2016**;35:6026-37.

28. Barretina J, Caponigro G, Stransky N, Venkatesan K, Margolin AA, Kim S, *et al*. The Cancer Cell Line Encyclopedia enables predictive modelling of anticancer drug sensitivity. *Nature* **2012**;483:603-7.

29. Medico E, Russo M, Picco G, Cancelliere C, Valtorta E, Corti G, *et al*. The molecular landscape of colorectal cancer cell lines unveils clinically actionable kinase targets. *Nat Commun* **2015**;6:7002.

30. Efron B, Tibshirani R. On testing the significance of sets of genes. *Ann Appl Stat* **2007**;1:107-29.

31. Hanzelmann S, Castelo R, Guinney J. GSVA: gene set variation analysis for microarray and RNA-seq data. *BMC Bioinformatics* **2013**;14:7.

32. Klijn C, Durinck S, Stawiski EW, Haverty PM, Jiang Z, Liu H, *et al*. A comprehensive transcriptional portrait of human cancer cell lines. *Nat Biotechnol* **2015**;33:306-12.

33. Julien S, Merino-Trigo A, Lacroix L, Pocard M, Goere D, Mariani P, *et al*. Characterization of a large panel of patient-derived tumor xenografts representing the clinical heterogeneity of human colorectal cancer. *Clin Cancer Res* **2012**;18:5314-28.

34. Hoshida Y. Nearest template prediction: a single-sample-based flexible class prediction with confidence assessment. *PLoS One* **2010**;5:e15543.

35. Puig I, Chicote I, Tenbaum SP, Arques O, Herance JR, Gispert JD, *et al*. A personalized preclinical model to evaluate the metastatic potential of patient-derived colon cancer initiating cells. *Clin Cancer Res* **2013**;19:6787-801.

36. Pemovska T, Kontro M, Yadav B, Edgren H, Eldfors S, Szwajda A, *et al*. Individualized systems medicine strategy to tailor treatments for patients with chemorefractory acute myeloid leukemia. *Cancer Discov* **2013**;3:1416-29.

37. Yadav B, Pemovska T, Szwajda A, Kulesskiy E, Kontro M, Karjalainen R, *et al*. Quantitative scoring of differential drug sensitivity for individually optimized anticancer therapies. *Sci Rep* **2014**;4:5193.

38. Nishida N, Nagahara M, Sato T, Mimori K, Sudo T, Tanaka F, *et al*. Microarray analysis of colorectal cancer stromal tissue reveals upregulation of two oncogenic miRNA clusters. *Clin Cancer Res* **2012**;18:3054-70.

39. He S, Smith DL, Sequeira M, Sang J, Bates RC, Proia DA. The HSP90 inhibitor ganetespib has chemosensitizer and radiosensitizer activity in colorectal cancer. *Invest New Drugs* **2014**;32:577-86.

40. Mendillo ML, Santagata S, Koeva M, Bell GW, Hu R, Tamimi RM, *et al*. HSF1 drives a transcriptional program distinct from heat shock to support highly malignant human cancers. *Cell* **2012**;150:549-62.

41. Wang H, Lu M, Yao M, Zhu W. Effects of treatment with an Hsp90 inhibitor in tumors based on 15 phase II clinical trials. *Mol Clin Oncol* **2016**;5:326-34.

42. Cercek A, Shia J, Gollub M, Chou JF, Capanu M, Raasch P, *et al*. Ganetespib, a novel Hsp90 inhibitor in patients with KRAS mutated and wild type, refractory metastatic colorectal cancer. *Clin Colorectal Cancer* **2014**;13:207-12.

43. Bendell JC, Jones SF, Hart L, Pant S, Moyhuddin A, Lane CM, *et al*. A phase I study of the Hsp90 inhibitor AUY922 plus capecitabine for the treatment of patients with advanced solid tumors. *Cancer Invest* **2015**;33:477-82.

44. Nagaraju GP, Alese OB, Landry J, Diaz R, El-Rayes BF. HSP90 inhibition downregulates thymidylate synthase and sensitizes colorectal cancer cell lines to the effect of 5FU-based chemotherapy. *Oncotarget* **2014**;5:9980-91.

45. McNamara AV, Barclay M, Watson AJ, Jenkins JR. Hsp90 inhibitors sensitise human colon cancer cells to topoisomerase I poisons by depletion of key anti-apoptotic and cell cycle checkpoint proteins. *Biochem Pharmacol* **2012**;83:355-67.

46. Piper PW, Millson SH. Mechanisms of resistance to Hsp90 inhibitor drugs: a complex mosaic emerges. *Pharmaceuticals (Basel)* **2011**;4:1400-22.

47. Ahmed D, Eide PW, Eilertsen IA, Danielsen SA, Eknæs M, Hektoen M, *et al*. Epigenetic and genetic features of 24 colon cancer cell lines. *Oncogenesis* **2013**;2:e71.

48. Mouradov D, Sloggett C, Jorissen RN, Love CG, Li S, Burgess AW, *et al*. Colorectal cancer cell lines are representative models of the main molecular subtypes of primary cancer. *Cancer Res* **2014**;74:3238-47.

49. Berg KCG, Eide PW, Eilertsen IA, Johannessen B, Bruun J, Danielsen SA, *et al*. Multi-omics of 34 colorectal cancer cell lines - a resource for biomedical studies. *Mol Cancer* **2017**;16:116.

50. Schutte M, Risch T, Abdavi-Azar N, Boehnke K, Schumacher D, Keil M, *et al*. Molecular dissection of colorectal cancer in pre-clinical models identifies biomarkers predicting sensitivity to EGFR inhibitors. *Nat Commun* **2017**;8:14262.

Table 1. Prediction accuracy of the cancer cell-adapted CMS classifier in primary CRCs

Patient series	Analysis platform	Samples classified by both CMS classifiers	Reference subtype	Cancer cell-adapted CMS classifier				Prediction accuracy [95% CI]
				CMS1	CMS2	CMS3	CMS4	
TCGA test-set (n = 143)[a]	RNA sequencing	91 (64%)	CMS1	12	0	0	0	85% [76%-91%]
			CMS2	1	34	1	6	
			CMS3	4	0	10	0	
			CMS4	0	1	1	21	
GSE14333 (n = 157)[a]	Affymetrix HG U133 Plus 2.0 arrays	116 (74%)	CMS1	15	0	2	1	86% [79%-92%]
			CMS2	1	34	5	3	
			CMS3	3	0	17	0	
			CMS4	1	0	0	34	
In-house patients (n = 208)[b]	Affymetrix HTA 2.0 arrays	165 (78%)	CMS1	36	0	1	0	92% [87%-96%]
			CMS2	0	66	2	1	
			CMS3	1	7	18	0	
			CMS4	0	1	0	32	
In-house patients (n = 201)[b]	Affymetrix Human Exon 1.0 ST arrays	138 (69%)	CMS1	22	0	1	3	87% [80%-92%]
			CMS2	0	49	3	2	
			CMS3	4	5	18	0	
			CMS4	0	0	0	31	

[a]Reference CMS classes obtained from Guinney *et al*. (21) [b]Reference CMS classes obtained using the RF predictor implemented in the R package CMSclassifier.

Table 2. Differential drug sensitivity between CMS1/4 and CMS2/3 cell lines

Drug[a]	Average difference in DSS[b]	P-value	FDR	Molecular targets/mechanisms
PF-03758309	10.8	8×10^{-4}	8×10^{-3}	PAK inhibitor
Rigosertib	10.5	4×10^{-4}	6×10^{-3}	PLK1 inhibitor
Disulfiram	9.0	3×10^{-3}	1×10^{-2}	Alcohol dehydrogenase inhibitor
YM155	9.0	3×10^{-3}	1×10^{-2}	Survivin inhibitor
Tipifarnib	8.8	1×10^{-3}	9×10^{-3}	Farnesyltransferase inhibitor
Luminespib	8.3	1×10^{-4}	4×10^{-3}	HSP90 inhibitor
Ganetespib	8.1	3×10^{-5}	2×10^{-3}	HSP90 inhibitor
Idarubicin	7.9	4×10^{-4}	6×10^{-3}	Topoisomerase II inhibitor
Teniposide	7.8	2×10^{-3}	1×10^{-2}	Topoisomerase II inhibitor
Indibulin	7.4	8×10^{-4}	8×10^{-3}	Mitotic inhibitor; microtubule depolymerizer
Dactinomycin	7.2	4×10^{-3}	2×10^{-2}	RNA and DNA synthesis inhibitor
Clofarabine	7.2	3×10^{-3}	1×10^{-2}	Anti-metabolite; Purine analog
Danusertib	7.1	6×10^{-3}	2×10^{-2}	Aurora, Ret, TrkA, FGFR-1 inhibitor
2-methoxyestradiol	7.0	1×10^{-4}	4×10^{-3}	Angiogenesis inhibitor
Radicicol	6.8	7×10^{-4}	8×10^{-3}	HSP90 inhibitor
Cytarabine	6.7	4×10^{-3}	2×10^{-2}	Anti-metabolite, interferes with DNA synthesis
Gemcitabine	6.6	1×10^{-2}	4×10^{-2}	Antimetabolite; Nucleoside analog
PHA-793887	6.4	2×10^{-3}	1×10^{-2}	CDK inhibitor
Valrubicin	6.4	2×10^{-3}	1×10^{-2}	Topoisomerase II inhibitor
8-chloro-adenosine	5.9	9×10^{-4}	8×10^{-3}	Nucleoside analog; RNA synthesis inhibitor

[a]Top 20 drugs (FDR from independent samples t-tests below 0.05) sorted by average difference in DSS values between CMS1/CMS4 (n = 15) and CMS2/CMS3 (n = 14) cell lines. [b]Positive values indicate drugs with strongest effect in CMS1/CMS4 cell lines.

Figures

Figure 1. Validation of molecular and clinicopathological characteristics of the CMS groups in primary CRCs

a) From a consecutive series of 409 patients with stage I-IV CRC, totally 323 (79%) tumors were confidently assigned to a CMS group (posterior probability larger than 0.5 from the random forest CMS classifier), while 46 tumors (11%) displayed mixed characteristics between two of the subtypes (posterior probability larger than 0.3 for both subtypes) and 40 tumors (10%) were indeterminate. Among the confidently classified tumors, known associations with the CMS groups were validated for b) MSI status, *BRAF* mutations, *KRAS* mutations and *TP53* mutations, c) patient gender, tumor localization, tumor differentiation grade and cancer stage, and d) patient survival. Patients with CMS4 tumors had a 5-year relapse-free survival rate of 47% compared with 67% for patients with CMS1-3 tumors. e) Gene set expression enrichment analyses comparing tumors in each individual CMS group with the three others confirmed subtype-specific biological properties. In parts b-e, the color code is the same as indicated in part a.

Figure 2. CMS classification of CRC cell lines

a) Flowchart of development of the cancer cell-adapted CMS classifier. Candidate template genes with high relative expression in each CMS group were identified in CRCs from TCGA (left). Prior to CMS classification using Nearest Template Prediction (right), genes with low expression levels and/or expression variation in CRC cell lines and genes with high expression in the tumor microenvironment were filtered out (blue background). b) Confident CMS classification was obtained for 126 (85%) of 148 CRC cell lines from unique patients using the adapted CMS classifier, with similar distribution among the subtypes as for the consecutive patient series. The molecular and biological characteristics of the CMS groups were also recapitulated among the cell lines, as shown c) for MSI status, *BRAF* mutations, *KRAS* mutations and *TP53* mutations, as well as d) by gene set expression enrichment analyses.

Figure 3. Differential drug responses among CMS groups

High-throughput drug screening (filtered list of 241 of totally 459 drugs) of CRC cell lines (n = 29) revealed differential drug responses among the CMS groups. Each plot represents a comparison of two subtypes, as indicated, and each dot represents one drug. Selected drugs are colored according to molecular targets, as indicated.

Figure 4. Selective activity of HSP90 inhibitors in CMS1 and CMS4

a) High-throughput drug screening of CRC cell lines (n = 29) showed that CMS2 was more sensitive to EGFR and HER2 inhibitors than the three other CMS groups. b) Compared to CMS2 and CMS3, CMS1 and CMS4 cell lines were more sensitive to three HSP90 inhibitors (red; luminespib, ganetespib and radicicol), 2ME (green; combined angiogenesis and tubulin inhibitor), atorvastatin (dark blue; HMG-CoA reductase inhibitor), indibulin (pale blue; tubulin-inhibitor) and disulfiram (pink; inhibitor of alcohol dehydrogenase). c) A validation drug screen of five additional cell lines predicted to belong to the CMS1 or CMS4 groups (green and black cell lines are MSI+ and MSS, respectively) confirmed strong sensitivity (red) to HSP90 inhibitors, 2ME, atorvastatin and disulfiram in comparison to two CMS3 cell lines included in the validation screen, as well as in comparison to the mean sensitivity in CMS2 and CMS3 cell lines in the initial screen. d) Three CMS4 cell lines with response to HSP90 inhibition (CACO2, LIM2099 and SW480) were treated with luminespib or DMSO (control). Paired differential gene expression analysis showed up-regulation of several members of the HSP family after HSP90 inhibition. e) In CMS4 PDX models (n = 34) of a liver metastasis from a chemotherapy-naïve CRC patient, combined administration of 5-FU and luminespib showed stronger anti-tumor activity than single agent treatment with 5-FU or luminespib, or in vehicle-treated controls. Tumor growth is plotted as the mean ± standard error of tumor volume fold changes of all mice per treatment arm at the indicated time points. No significant changes in Ki67 protein expression in post-treatment samples (relative to vehicle-treated controls) confirmed that the CMS4 model was chemoresistant, while increased expression of HSP70 after luminespib treatment showed a targeted effect of HSP90 inhibition (P-values were calculated by Welch's t-test; sample numbers vary due to availability of high-quality samples or data). f) CMS2 PDX models (n = 34) were highly chemosensitive, as shown by a strong anti-tumor activity of 5-FU monotherapy and reduced

Ki67 expression in post-treatment samples, and there was no synergistic effect of combining 5-FU with luminespib. In contrast with the *in vitro* data, luminespib monotherapy had a moderately stronger anti-tumor activity in CMS2 (relative to vehicle-treated controls) than in CMS4, but this was not associated with changes in HSP70 expression in CMS2 post-treatment samples.

Figure 1

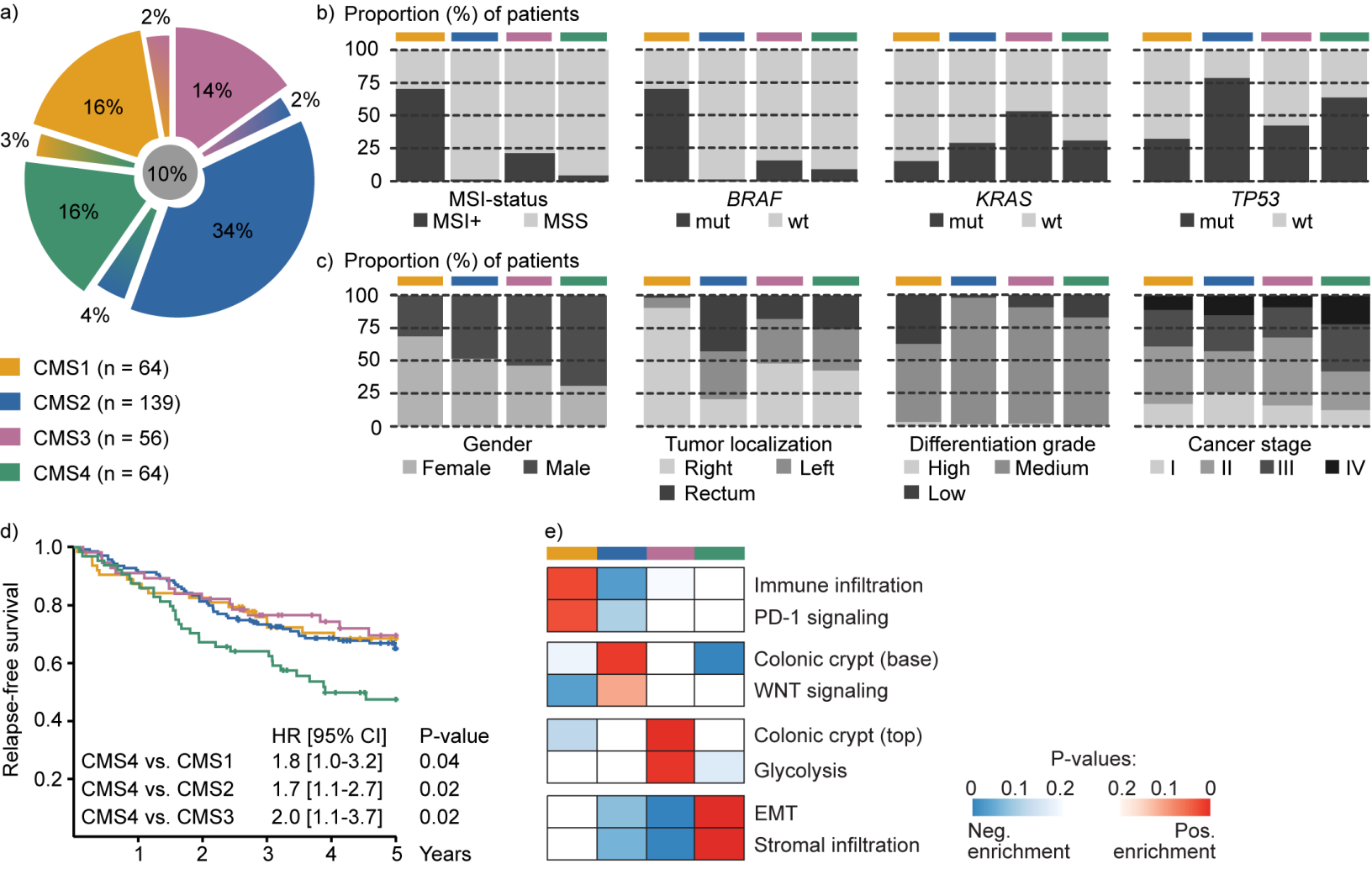

Figure 2

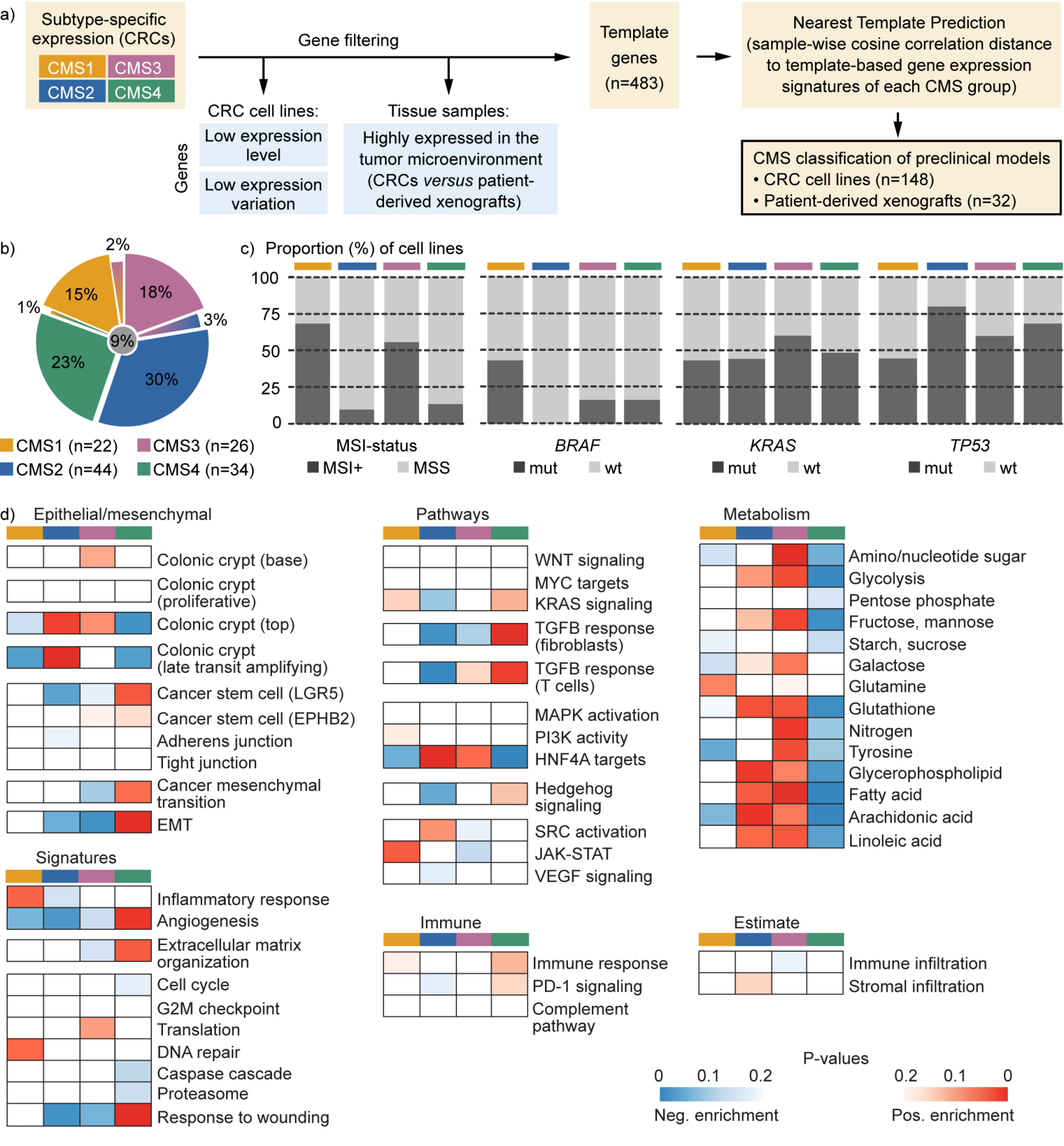

Figure 3

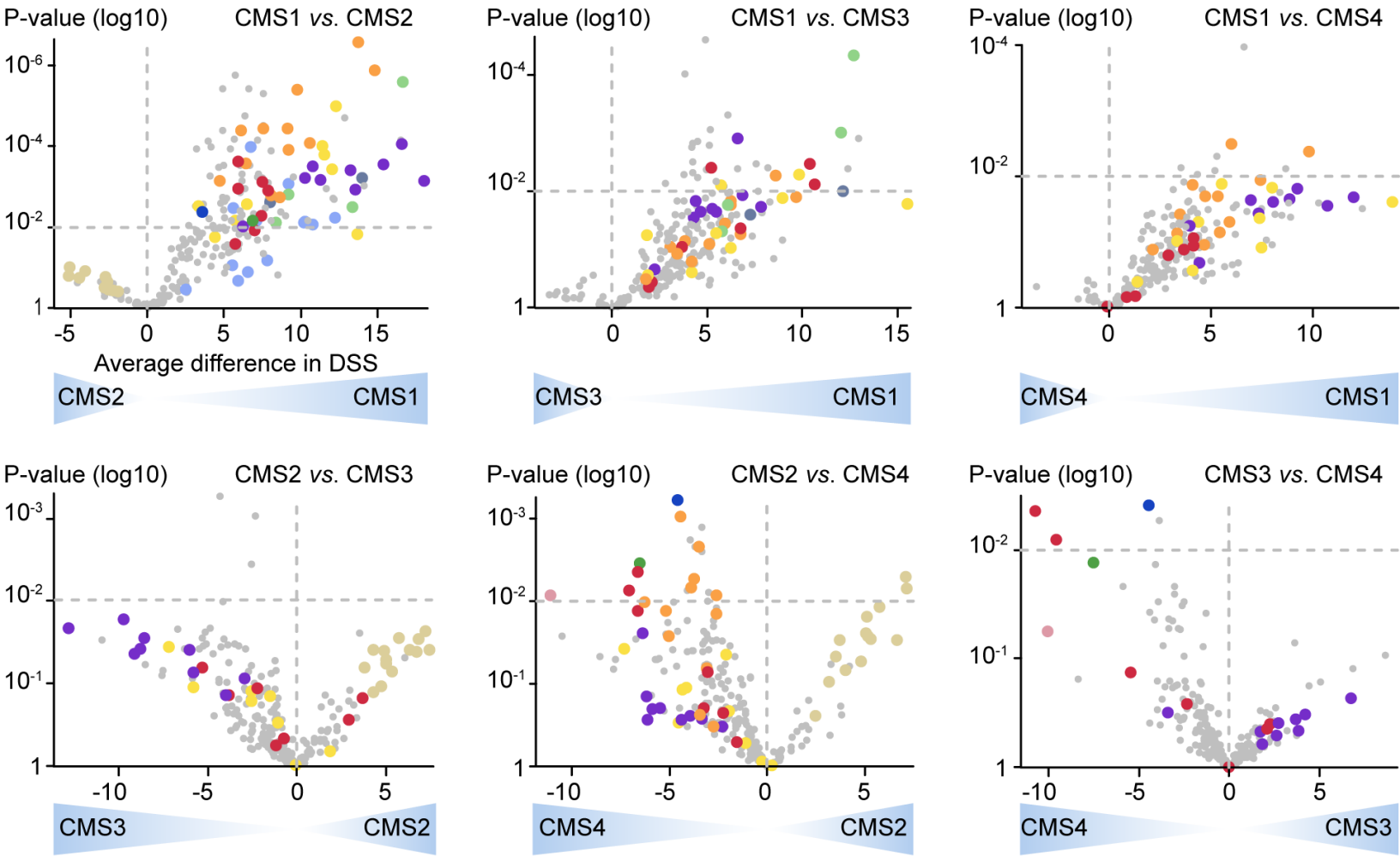

Topoisomerase inhibitors
Anti-metabolites
Mitotic inhibitors
HSP90 inhibitors
EGFR/HER2 inhibitors
Angiogenesis/tubulin inhibitor
PLK1 inhibitor
Aurora/pan-aurora inhibitors
HMG-CoA-reductase inhibitor
Alcohol dehydrogenase inhibitor
Farnesyl transferase inhibitors

Figure 4

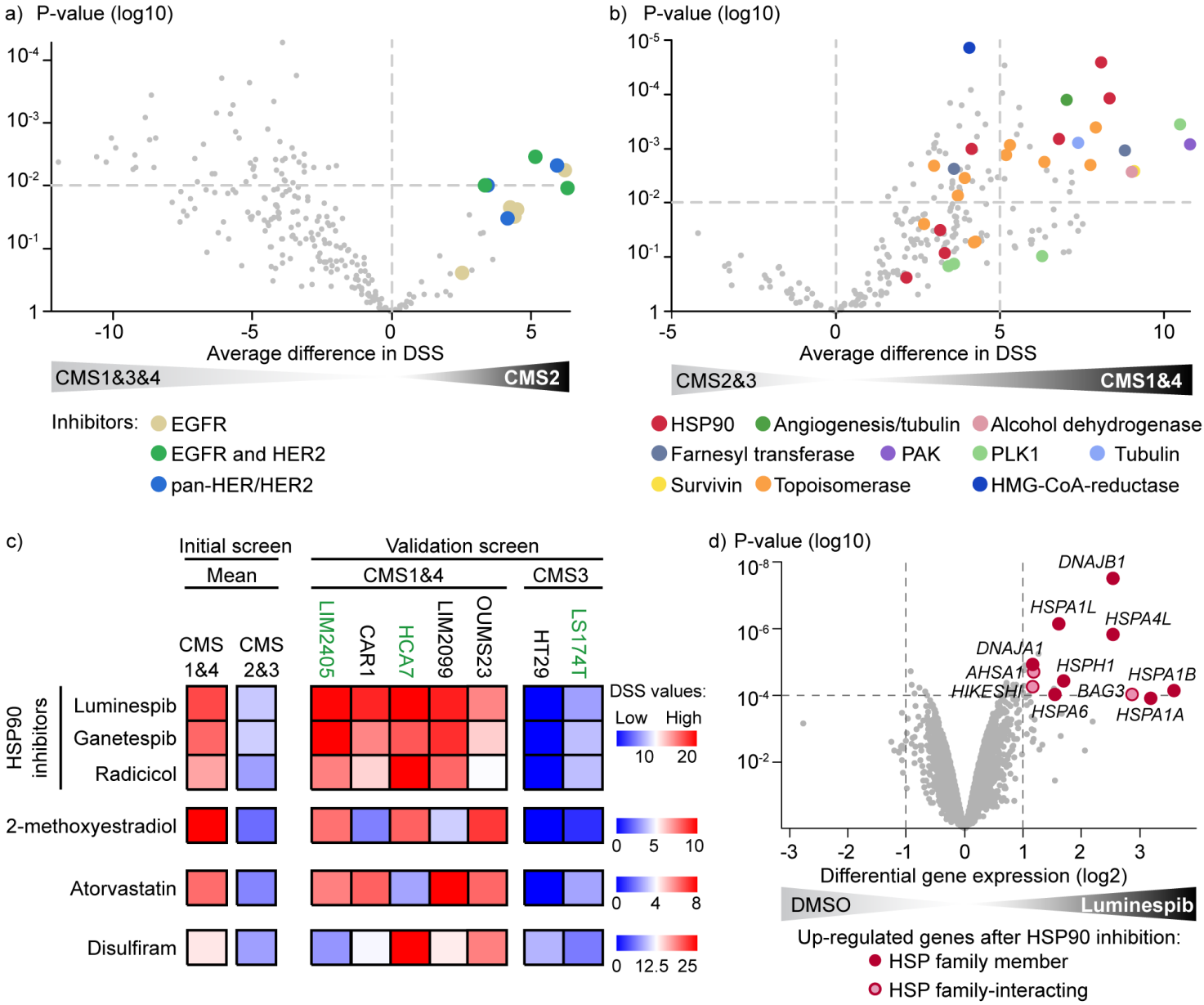

CMS4 PDX models (MSS, *KRAS*/*NRAS* wt, *BRAF*^{V600E} mut):

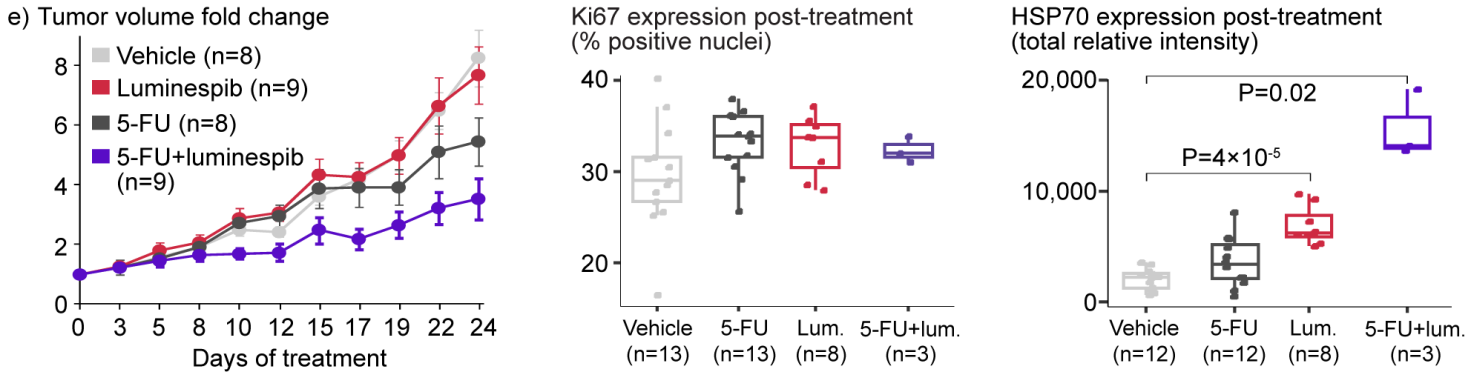

CMS2 PDX models (MSS, *KRAS*/*NRAS*/*BRAF* wt, *TP53* mut):

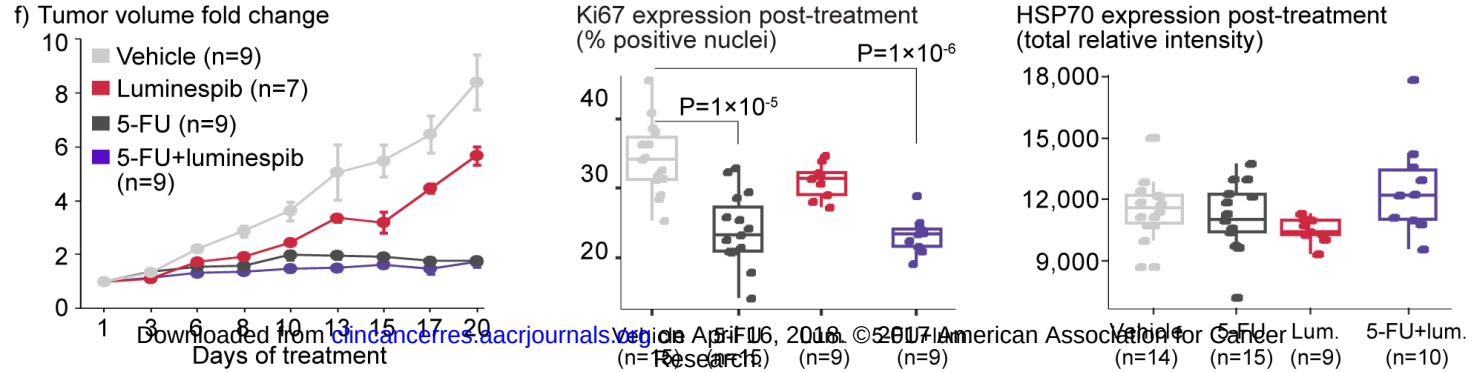

AACR American Association for Cancer Research

Clinical Cancer Research

Colorectal cancer Consensus Molecular Subtypes translated to preclinical models uncover potentially targetable cancer-cell dependencies

Anita Sveen, Jarle Bruun, Peter W Eide, et al.

Clin Cancer Res Published OnlineFirst December 14, 2017.